

# Low-temperature chemical vapor deposition of tantalum nitride from tantalum pentabromide for integrated circuitry copper metallization applications

Xiaomeng Chen, Gregory G. Peterson, Cindy Goldberg, Gerry Nuesca, Harry L. Frisch, and Alain E. Kaloyeros<sup>21</sup>

*New York State Center for Advanced Thin Film Technology and Department of Physics, The University at Albany—State University of New York, Albany, New York 12222*

Barry Arkles

*Gelest Inc., Tullytown, Pennsylvania 19007*

John Sullivan

*MKS Instruments Inc., Andover, Massachusetts 01810*

(Received 14 April 1998; accepted 6 November 1998)

A low-temperature (<450 °C) thermal chemical vapor deposition (CVD) process was developed for the growth of TaN<sub>x</sub> from the reaction of tantalum pentabromide, ammonia, and hydrogen. Studies of process reaction kinetics yielded two sequential rate-controlling steps, with an activation energy of 0.45 eV for the kinetically limited reaction regime. Additionally, a systematic design of experiments approach examined the effects of key process parameters, namely, substrate temperature, source temperature, and hydrogen and ammonia flows, on film properties. A wide CVD process window was established for nitrogen-rich amorphous TaN<sub>x</sub> with contamination below 1 at.%. Film conformality was higher than 95% in nominally 0.30 μm, 4.5:1 aspect ratio, trench structures.

## I. INTRODUCTION

Copper (Cu) is being evaluated and implemented as a highly viable interconnect material for ultra-large-scale integration (ULSI), due to its lower resistivity and superior resistance to electromigration as compared to the more commonly used aluminum (Al) and its alloys.<sup>1</sup> In this respect, a critical need exists for the identification and development of diffusion barrier liners for emerging Cu-based metallization schemes to isolate Cu from the dielectric and device regions of the chip. These liners are required to prevent undesirable diffusion and interaction phenomena, which could lead to reliability problems and device failure. They must also be able to withstand repeated thermal processing, and serve as strong adhesion promoters to ensure the integrity of the various metallization layers needed.<sup>2</sup>

Various material systems, such as refractory metals, their nitrides, and ternary metal-silicon-nitrogen compounds, have been examined for such applications.<sup>3</sup> Of these materials, titanium and tantalum nitrides, and their ternary compounds, are among the most extensively investigated. TiN is widely used in current aluminum- and tungsten-based interconnections as a diffusion barrier. However, the effectiveness of TiN as a Cu diffusion barrier still needs to be documented. Additionally, when

using TiN as a diffusion barrier, it effectively requires Ti/TiN bilayered structure. Adding a Ti layer underneath the TiN is necessary to lower contact resistance and improve adhesion between TiN and the underlying Si.<sup>4</sup> Considering the need for progressively thinner liners to maximize space availability for the actual conductor in the continuously shrinking device structures, the use of Ti/TiN stacks might be increasingly prohibitive as device features shrink below quarter micron. Ta-based compounds provide a potential solution to these problems. Tantalum and its nitrides are highly refractory materials which are stable to extremely high temperatures.<sup>5</sup> More importantly, tantalum and its nitrides are known to be thermodynamically stable with respect to Cu, because of the absence of Cu-Ta or Cu-N compounds. For instance, a sputtered Ta thin barrier with 50 nm thickness has demonstrated its resistance to Cu diffusion up to 550 °C for 1 h.<sup>6</sup> Tantalum nitrides could provide even greater resistance to diffusion relative to the pure metal, in view of their dense interstitial crystalline structure.<sup>7</sup> As a result, sputtered tantalum nitrides have been successfully demonstrated as good diffusion barriers for Cu technology, with proven Cu-TaN contact stability to temperatures as high as 750 °C.<sup>3</sup>

Sputtering in its various forms, including collimated and ionized sputtering, has been successfully implemented for the deposition of Ta and its nitrides. However, as feature sizes of devices and interconnects are

<sup>21</sup>Address all correspondence to this author.

reduced below quarter micron, these techniques might produce nonconformal coverage, primarily at the bottom corners of vias and trenches. Additionally, sputtered Ta might be difficult to integrate with various low dielectric constant materials, in view of the structural and chemical damage that could be induced by the heavy Ta ions into the fragile dielectric matrix. Chemical vapor deposition, on the other hand, is an attractive alternative, especially in terms of its inherent ability to provide highly conformal deposition in aggressive device topographies. In this respect, the availability of low-temperature CVD processing represents a viable route to the integration of Ta liners with thermally sensitive dielectric materials. Earlier attempts at CVD Ta and TaN<sub>x</sub> employed mostly TaCl<sub>5</sub> as a precursor.<sup>8</sup> However, the high deposition temperature (>600 °C) required seriously limited its usefulness. Other efforts on metalorganic CVD (MOCVD) of TaN<sub>x</sub> used various precursors including the dialkylamido Ta complex,<sup>9</sup> Ta(NEt)(NEt<sub>2</sub>)<sub>2</sub>/Ta(η<sup>2</sup>EtN = CMeH)(NEt<sub>2</sub>)<sub>3</sub> blend,<sup>10</sup> and Ta = NBu'(NEt<sub>2</sub>)<sub>3</sub>,<sup>11</sup> etc. Unfortunately, various serious challenges, such as high deposition temperature (>500 °C), the inclusion of hydrogen concentrations of up to 40%, and the incorporation of several atomic percent of C and O minimized their technological usefulness.

In view of these issues, it is clear that there is a need for a low-temperature (<450 °C) thermal CVD process for the growth of pure, ultrathin (<250 Å) films of tantalum and its nitride with viable electrical and barrier properties, for incorporation in the 0.18 μm device generation and beyond. Accordingly, our work has focused on the development and demonstration of such technology.

One of the most important ingredients in achieving this goal is the identification of an appropriate source precursor. Our strategy involved the use of simple inorganic tantalum compounds in which the dissociation energy of primary bonds is relatively low and recombination can be interrupted by the presence of hydrogen or nitrogen to yield, respectively, tantalum or tantalum nitrides. Tantalum pentabromide (TaBr<sub>5</sub>), which belongs to the same class of halide chemistries as TaCl<sub>5</sub>, was selected as the source precursor because of bonding energy considerations. The Ta–Br bond strength is ~28.6 kcal/mol, as compared to ~41 kcal/mol for Ta–Cl,<sup>12</sup> implying that TaBr<sub>5</sub> could potentially decompose at significantly lower temperature than TaCl<sub>5</sub>. Additionally, the activation energy for bromine diffusion is expected to be higher than chlorine, given that Br is much heavier than Cl. This expectation is supported by studies of the interaction of fluorine and chlorine with silicon (111),<sup>13</sup> which showed that the barrier for chlorine penetration into the silicon surface is much larger than that for

fluorine. This behavior was attributed to the larger size, and hence higher ionicity and resulting coulomb interaction, of the chlorine atom in comparison with its fluorine counterpart. Similar findings were reported for the diffusion characteristics of iodine and chlorine from TiN films formed by thermal chemical vapor-deposition (TCVD) from the halide precursors tetraiodotitanium (TiI<sub>4</sub>) and tetrachlorotitanium (TiCl<sub>4</sub>).<sup>14</sup> These studies indicate that for residual Br in the deposited films, the thermal energy required to initiate Br diffusion is higher than in the case of Cl. This feature is highly desirable given the adverse effects, including corrosion, that halides out-diffusion from the barrier layer could induce in the actual copper conductor.

In this paper, results are presented from a two-stage study that developed and optimized a low temperature TCVD TaN<sub>x</sub> process using NH<sub>3</sub> and H<sub>2</sub> as co-reactants. The first stage of this study focused on examining the reaction kinetics that drive the TCVD process, leading to the establishment of a fundamental understanding of process rate-limiting steps. In a second stage, a systematic design of experiments (DOE) modeling approach was implemented in a detailed investigation of the effects of key process parameters on film properties, leading to the identification of an optimized process window for the growth of TaN<sub>x</sub>. The two stages of our study are described below, along with a description of primary experimental conditions, a discussion of key experimental findings, and a presentation of pertinent conclusions.

## II. EXPERIMENTAL DETAILS

### A. Description of CVD reactor and associated processing conditions

Process development was performed in a custom-designed, 5" wafer, warm wall, plasma capable, stainless steel CVD reactor. The specific reactor geometry has been reported elsewhere, and will only be summarized here.<sup>15</sup> A standard pressure-based bubbler unit was applied to the delivery of the solid TaBr<sub>5</sub> precursor. The unit was attached to a cone-shaped shower head of the CVD reactor through a special delivery line which was equipped with two high-vacuum, high-temperature valves to allow precursor delivery to either the processing chamber or, through a bypass line, directly to the pumping unit. The use of a bypass line allowed both the establishment of a steady-state precursor flux prior to introduction into the chamber, and preconditioning of the sublimator prior to actual delivery into the reactor. Hydrogen gas was used as carrier gas to aid in precursor delivery. A T-shaped adapter at the top of the shower head connected both the precursor and reactant delivery lines to the processing module.

The substrates were loaded on a heater chuck which consisted of a quartz plate placed on an electrically isolated borolectric heater. The heater backside was purged with 50 sccm of argon (Ar) to prevent undesirable diffusion of reactive processing gases and chemical reactants. Substrate temperature was determined by calibrating the power supplied to the heater as a function of substrate temperature with a specially designed sensor wafer prior to actual processing. A plasma mesh was installed between the cone type shower head and substrate to act as active electrode in a parallel plate diode type plasma configuration.

Symmetrical pumping of the reactor was achieved by pumping through four lines at the bottom of the chamber. Pressure control in the chamber under a given flow of process gases was achieved by manual throttle of a high vacuum gate valve. The system was equipped with a CTI-cryogenics model cryo-Torr 8 Cryopump, which is capable of achieving a base pressure of  $10^{-6}$  Torr, to ensure reactor cleanliness prior to deposition runs. Alternatively, a mechanical pump was used during actual processing. An MKS baratron pressure gauge and an HPS cold cathode gauge monitored reactor base and process pressures.

A load lock was used to prevent atmospheric contamination of the deposition chamber. The load lock was isolated from the reactor by an electrically controlled gate valve. The load lock was evacuated using a model TCP 121 turbomolecular pump package to a base pressure in the  $10^{-6}$  Torr range. The pressure in the load lock was monitored with an HPS model 421 cold cathode gauge. Wafer transfer was achieved with a manual, magnetically controlled, load lock arm.

The substrates used for these experiments were nonpatterned silicon and silicon dioxide, and SEMATECH patterned silicon dioxide structures with nominal  $0.30 \mu\text{m}$ , 4.5 to 1, aspect ratio structures. Prior to deposition, all samples received a standard organic clean process consisting of a one minute bath in trichloroethylene, acetone, and then methanol. The substrates were subsequently dried in a stream of argon gas. Finally, the silicon samples were dipped into a 10% hydrofluoric acid solution for 1 min and then rinsed in de-ionized wafer, to remove the native oxide. After the silicon samples were dried by argon again, all the samples were then immediately mounted on a 5 in. carrier wafer and loaded into the reactor via the load lock to minimize atmospheric contamination. A soft hydrogen plasma predeposition clean was performed on all samples.

## B. DOE approach

A systematic approach was implemented in the development and optimization of the CVD TaN<sub>x</sub> process. It consisted of implementing a DOE study which em-

ployed the RS-1 Discover software to plan and execute deposition experiments and develop optimized CVD process windows in the most efficient way possible. Traditional experimentation consists of varying the CVD process parameters in an unsystematic fashion, with the results of one run being analyzed to define the parameters for the next run. This approach is not only time-consuming but might also be misleading, especially in cases where the optimum CVD process window is too narrow to be identified by a trial and error approach. The RS-1 software supports instead a systematic, four-stage approach which involves data organization, data visualization, statistical analysis, and interpretation of statistical analysis.

In a DOE study, two sets of actual CVD deposition runs are performed. The first, known as screening DOE, is designed to identify the relative effect of the various CVD process parameters on TaN<sub>x</sub> film quality and performance. Based on the results of the screening DOE, a second set of expanded CVD deposition runs, known as full DOE, are performed to identify optimum sets of processing conditions for the growth of TaN<sub>x</sub> films with the desired performance and characteristics.

The full DOE approach explored the effects of four key process parameters, namely, substrate temperature, source temperature, hydrogen carrier gas flow rate, and ammonia reactant gas flow rate, on key film characteristics including growth rate, composition, resistivity, and texture. The full DOE study was conducted using a response surface model (RSM) to map the entire process parameter space. The RSM model included quadratic terms and was generated from a center composite face (CCF) design. In the CCF design, each process parameter (predictor) is varied among three values: a minimum value, a maximum value, and a center point. Table I displays the predictor ranges used in our study. The corresponding total number of actual experimental deposition runs was 25 in this case. Additionally, the center point was repeated seven times to determine reproducibility, which was found to be better than 90%. This resulted in a total of 32 DOE experimental deposition runs. As such, the CCF design allows accurate determination of the dependence of film properties (response) on key process parameters (predictors), including quadratic type dependencies.

TABLE I. Predictor ranges used in the DOE study for the development of TCVD TaN<sub>x</sub>.

Process parameter (predictor)	Low value	Center value	High value
Source temperature (°C)	150	160	170
Substrate temperature (°C)	350	425	500
H <sub>2</sub> flow (sccm)	30	45	60
NH <sub>3</sub> flow (sccm)	300	450	600

### C. Characterization techniques

The resulting TaN<sub>x</sub> films, with a thickness ranging from ~20 to 200 nm depending on the experimental conditions, were subsequently characterized by Auger electron spectroscopy (AES), x-ray photoelectron spectroscopy (XPS), atomic force microscopy (AFM), x-ray diffraction (XRD), Rutherford backscattering spectrometry (RBS), hydrogen profiling, four point resistivity probe, transmission electron microscopy (TEM), scanning electron microscopy (SEM), and cross-sectional SEM (CS-SEM).

Compositional and microchemical information was obtained by AES, RBS, hydrogen profiling, and XPS. In these studies, the results were standardized using a physical vapor deposition (PVD) TaN<sub>x</sub> where *x* was calibrated by a wavelength dispersive electron microprobe technique. In addition, RBS was applied in conjunction with CS-SEM in the determination of film thickness and average growth rate. Alternatively, XRD, TEM, and AFM were applied to examine film texture and bulk and surface grain size and morphology. Deposition rates were defined as  $T/t$  where  $T$  is film thickness and  $t$  is run time.

## III. RESULTS AND DISCUSSION

### A. Study of reaction kinetics

A reaction kinetics study was performed by investigating the dependence of growth rate on substrate temperature. For this purpose, substrate temperature was varied between 350 and 500 °C, while all other process parameters were kept constant, including 160 °C source temperature, 45 sccm H<sub>2</sub> flow, 450 sccm NH<sub>3</sub> flow, and 0.96 Torr reactor pressure. Figure 1 displays the corresponding Arrhenius plot of  $\ln(\text{growth rate})$  versus  $1/T$ .

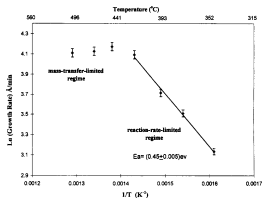


FIG. 1. Arrhenius plot of  $\ln(\text{growth rate})$  as a function of deposition temperature.

At temperatures below 425 °C, the Arrhenius plot shows a steep linear slope, indicating the dominance of a single reaction rate-limiting mechanism, with an activation energy of reaction of 0.45 eV. In this regime, film growth rates ranged from 2.5 to 7.5 nm/min within the process window investigated. At temperatures above 425 °C, the Arrhenius plot shows a significantly more leveled behavior, corresponding to a mass transfer limiting mechanism. In this regime, film growth rates leveled ~7.5 nm/min for the process window investigated. As shown in the following sections, film structural characteristics change once the threshold is crossed between the two regimes. Additionally, a trend of decreasing growth rate is observed with increasing substrate temperature in the mass transport regime. This may be potentially attributed to partial precursor decomposition prior to reaching the substrate in this higher temperature regime, leading to a net decrease in precursor concentration at the substrate surface.

### B. Effects of key process parameters on film properties

#### 1. Effects of process parameters on growth rate

Figures 2 and 3 display the dependence of TaN<sub>x</sub> growth rates on key predictors for deposition on Si substrates. Within the DOE predictor space investigated, growth rates ranged from 3.5 to 11 nm/min.

In particular, Fig. 2 displays the dependence of growth rate on substrate temperature and H<sub>2</sub> flow rate at 300 sccm NH<sub>3</sub> flow rate and 167 °C source temperature. Alternatively, Fig. 3 shows the dependence of growth rate on source temperature and NH<sub>3</sub> flow rate at 60 sccm H<sub>2</sub> flow rate and 470 °C substrate temperature. The main behavioral trends observed are:

(i) Within the parameter space investigated, growth rate exhibited two distinct modes of dependence on substrate temperature. At substrate temperature below ~420 °C, an exponential dependence was observed with

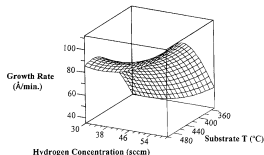


FIG. 2. DOE plot of growth rate as a function of substrate temperature and H<sub>2</sub> concentration, at 300 sccm NH<sub>3</sub> flow and 167 °C source temperature.

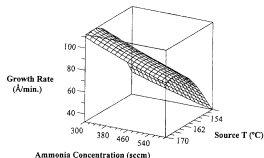


FIG. 3. DOE plot of growth rate as a function of source temperature and  $\text{NH}_3$  concentration, at 60 sccm  $\text{H}_2$  flow and 470 °C substrate temperature.

growth rate increasing significantly with higher substrate temperature. However, at substrate temperature above  $\sim 450$  °C, growth rate became mostly independent of variation in substrate temperature. This behavior is consistent with the observation of two sequential rate-limiting steps in the reaction kinetics study reported in the previous section. Both the reaction rate-limited regime ( $T_{\text{substrate}} < \sim 420$  °C) and mass transfer limited regime ( $T_{\text{substrate}} > \sim 450$  °C) are clearly observed in this DOE model.

(ii) The growth rate was also highly dependent on source temperature. A source temperature increase of  $\sim 16\%$  from 150 to 165 °C caused a growth rate enhancement of  $\sim 130\%$ , from  $\sim 35$  to  $\sim 80$  Å/min. The growth rate tended to level off as source temperature exceeded 165 °C. This behavior could be attributed to an increase in precursor partial pressure in the reaction zone at higher source temperature, leading to an enhancement in reaction probability, and resulting in a higher growth rate. Precursor partial pressure appears to saturate the decomposition reaction at source temperatures higher than 165 °C, leading to constant growth rates.

(iii)  $\text{NH}_3$  flow rate appeared to have a strong effect on growth rate. It was observed that growth rate decreased significantly with increasing  $\text{NH}_3$  flow rate. This trend could be due to either a reduction in precursor residence time in the reactor at higher  $\text{NH}_3$  flows, leading to lower reaction probability, or the saturation of substrate surface sites by  $\text{NH}_3$  intermediates, which could inhibit adsorption and decomposition of the precursor.

(iv)  $\text{H}_2$  carrier gas flow rate also exhibited some expected effects on growth rate. An increase in growth rate from  $\sim 35$  to  $\sim 55$  Å/min was observed with increasing  $\text{H}_2$  flow from  $\sim 40$  to 60 sccm.  $\text{H}_2$  concentration showed no effect on growth rate at  $\text{H}_2$  flow rates below  $\sim 40$  sccm. This behavior is attributed to the higher precursor delivery rates into the reactor at increased carrier gas flows, leading to enhanced precursor partial

pressure in the reaction zone, and resulting in larger growth rates. However, variations in carrier gas flow rates have a less pronounced effect on precursor flux into the reactor as compared to source temperature, and hence lead to a smaller change in growth rates.

## 2. Effects of process parameters on Br contamination

Figures 4 and 5 display the dependence of Br concentration, measured using RBS, on key predictors in the DOE study. In particular, Fig. 4 shows variations in Br concentration as a function of substrate temperature and  $\text{NH}_3$  concentration at a source temperature of 170 °C and  $\text{H}_2$  flow rate of 60 sccm. Alternatively, Fig. 5 displays Br concentration as a function of source temperature and  $\text{H}_2$  flow rate at a substrate temperature of 407 °C and  $\text{NH}_3$  flow rate of 600 sccm. In the process window investigated, the following trends are observed:

(i) Br concentration exhibited a strong dependence on substrate temperature. An increase in substrate temperature from 350 to 500 °C yielded a significant reduction in the Br concentration, from about 5 at.% to well below the detection limits of the analytical

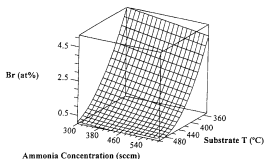


FIG. 4. DOE plot of Br concentration as a function of substrate temperature and  $\text{NH}_3$  concentration, at 170 °C source temperature and 60 sccm  $\text{H}_2$  flow.

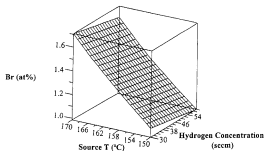


FIG. 5. DOE plot of Br concentration as a function of source temperature and  $\text{H}_2$  concentration, at 407 °C substrate temperature and 600 sccm  $\text{H}_2$  flow.

techniques employed (XPS and RBS). This behavior might be attributed to the availability of more thermal energy at higher substrate temperature, leading to a more efficient decomposition reaction as exhibited by complete cleavage of Ta–Br bonds. The achievement of TaN<sub>x</sub> film deposition with low Br contamination (<1 at.%) at low substrate temperatures (≤425 °C) is illustrated in Fig. 6, which exhibits a typical RBS spectrum, along with its simulation spectrum, for a thermal CVD TaN<sub>x</sub> film grown at 425 °C. RBS analysis yielded a Br concentration ~0.5 at.%.

(ii) Alternatively, Br concentration seemed to decrease very slowly with increasing NH<sub>3</sub> flow rate. However, the decrease in Br concentration as a function of NH<sub>3</sub> flow rate was below 10% regardless of the substrate temperature used. The decrease in Br concentration is well within the 10% experimental error of our DOE study, implying that Br concentration is independent of NH<sub>3</sub> flow rate in the process regime explored herein.

(iii) Br concentration exhibited a marked dependence on source temperature. For instance, a source temperature decrease of only 12%, from 170 to 150 °C, caused a Br concentration reduction of ~40%, from ~1.7 to ~1.0 at.%. This trend may be attributed to reduction in precursor partial pressure in the reaction zone at the lower source temperature, leading to a more efficient passivation of Br species by H<sub>2</sub> and NH<sub>3</sub> intermediates, and less Br incorporation in the resulting films.

(iv) Changes in H<sub>2</sub> flow within the process regime investigated showed no effects on Br concentration. Less than 5% decrease in Br concentration was seen for a 100% increase in the hydrogen flow rate, from 30 to

60 sccm. This variation of Br concentration is within the experimental error of the DOE, as discussed earlier.

### 3. Effects of process parameters on stoichiometry

Similarly, within the process regime under investigation, all films exhibited a constant N/Ta ratio throughout the film. N/Ta ratios varied between 1.75 and 1.87, depending on process parameters, as displayed in the AES spectrum of Fig. 7. Compositional variation was ~6.8%. This implies that within the experimental error of the DOE, N/Ta ratios are independent of process parameters in the predictor range investigated. It should be noted that within this predictor range explored herein, AES measurements showed that all films exhibited oxygen, carbon, and other light element contamination levels well below the AES detection limits, as illustrated in Fig. 7.

XPS measurements confirmed that the films were a tantalum nitride phase. The XPS N1s and 4f 1/2 core energy peak for the CVD-grown films, as shown typically in Fig. 8, were located at respectively,  $397.6 \pm 0.1$  and  $22.85 \pm 0.15$  eV, corresponding to the formation of tantalum nitride.<sup>16</sup>

### 4. Effects of process parameters on microstructure

The texture of TaN<sub>x</sub> films deposited within the process window investigated showed a strong dependence on substrate temperature. This is documented by XRD studies performed on samples grown throughout the DOE parameter space analyzed. As displayed in Fig. 9, it was observed that the films deposited at substrate temperatures below the DOE center set point value of the substrate temperature exhibited broad and weak reflection in XRD spectra, regardless of other processing conditions. In this respect, Figs. 9(a) and 9(b) correspond to films grown at, respectively, 350 and 425 °C. These broad and weak XRD reflection peaks suggest an amorphous TaN<sub>x</sub> phase, a conclusion

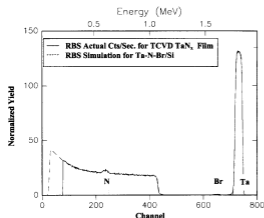


FIG. 6. RBS spectrum of a 120 nm-thick thermal CVD TaN<sub>x</sub> film grown at 425 °C substrate temperature, 45 sccm H<sub>2</sub>, 160 °C source temperature, and 600 sccm NH<sub>3</sub>.

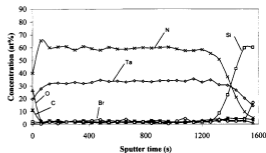


FIG. 7. AES depth profile of a 120 nm-thick thermal CVD TaN<sub>x</sub> film grown at 425 °C substrate temperature, 45 sccm H<sub>2</sub>, 160 °C source temperature, and 600 sccm NH<sub>3</sub>.

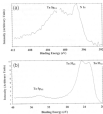


FIG. 5. XPS high-resolution scan for (a) Fe  $2p$  core peak, and (b) Ti  $2p$  core peak from a 100 nm-thick thermal CVD TiN film grown at 425 °C substrate temperature, 100 °C source temperature, and 400 sccm  $N_2$ .

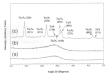


FIG. 6. XRD spectra of 100 nm-thick thermal TiN films grown at substrate temperatures of (a) 300 °C, (b) 425 °C, and (c) 500 °C. Other growth parameters included 45 sccm  $H_2$ , 100 °C source temperature, and 400 sccm  $N_2$ .

supported by TEM results. Neither grain boundaries nor a crystalline lattice could be detected in the high-resolution cross-section TEM image of the CVD TiN film as seen in Fig. 10(a). As expected, no diffraction spots, characteristic of periodic crystal structure, were detected using the Fast Fourier Transform method in

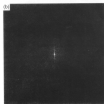
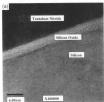


FIG. 7. (a) High-resolution cross-section TEM bright-field image, (b) corresponding Fast Fourier Transform (FFT) image, both taken for a 100 nm-thick thermal TiN film grown at 425 °C substrate temperature, 45 sccm  $H_2$ , 100 °C source temperature, and 400 sccm  $N_2$ .

from the corresponding TEM diffraction pattern shown in Fig. 8(b).

Alternatively, the films deposited at the maximum substrate temperature reported in the DOE study (500 °C) yielded typically an XRD spectrum consisting of a mixture of a dominant tetragonal TiN phase in co-existence with a hexagonal Ti<sub>2</sub>N phase, as demonstrated in Fig. 9(c).

Parameter	Typing of the
Substrate	Si(100)
Gas flow	500 sccm
Gas flow	1000 sccm
Gas flow	1000 sccm
Reaction time	100 min



FIG. 11. AFM image of a 100 nm-thick TiN film grown at 425 °C substrate temperature, 50 sccm  $H_2$ , 100 °C source temperature, and 500 sccm  $N_2$ .

In addition, AFM measurements demonstrate smooth and nonporous surface morphology with a typical non-monotony (RMS) surface roughness of 0.54 nm for a 1100 Å TiN film, as documented by the AFM image shown in Fig. 11.

### 5. Effects of process parameters on resistivity

Within the process regime investigated, film resistivity ( $\rho$ ) was primarily a function of substrate temperature. For films grown below 425 °C,  $\rho = (1.00 \pm 0.00) \times 10^2 \mu\Omega \text{ cm}$ . For films grown above 500 °C,  $\rho = (5.00 \pm 0.00) \times 10^2 \mu\Omega \text{ cm}$ . Between 425 and 500 °C, resistivity values varied between these two extremes, namely,  $(5.00 \pm 0.40) \times 10^2 < \rho < (1.00 \pm 0.00) \times 10^2 \mu\Omega \text{ cm}$ .

Resistivity values observed for the films deposited at 500 °C could be attributed to the existence of a mixed TiN phase consisting of hexagonal TiN and tetragonal  $Ti_2N_3$ , as determined by XRD. In this respect, the tetragonal  $Ti_2N_3$  has a resistivity  $\sim 6 \times 10^2 \mu\Omega \text{ cm}$ ,<sup>17</sup> while hexagonal TiN exhibits a resistivity of  $\sim 100 \mu\Omega \text{ cm}$ .<sup>17</sup> It is thus suggested that the high resistivity values in this case are primarily due to the presence of the  $Ti_2N_3$  phase.

Alternatively, the appreciably higher resistivities for films deposited below 425 °C might be attributed to a different reason. Potential factors include film stoichiometry, thickness, purity, and texture.<sup>18</sup> However, the TiN films deposited below 425 °C exhibited a similar stoichiometry to those deposited at 500 °C, as determined by AES and XPS. Thus, film stoichiometry was eliminated as a potential factor in the observed higher film resistivity at lower substrate temperatures. Similarly, the thicknesses of all films deposited in this DOE study were greater than 1000 Å. Accordingly,

surface wetting, which might cause such resistivity increase in ultrathin layers, was also disregarded as a key factor in the resistivity trends observed.

As for impurities, RBS and AES studies showed that all films contained less than 2 at.% Fe contamination, as discussed earlier. In particular, films deposited at 350, 425, and 500 °C contained, respectively, <0.5, 0.1, and <0.2 at.% Fe. Similarly, H, C, and O contamination in the films was below the detection limits of hydrogen profiling, AES, and XPS. It is therefore argued that Fe, C, and O contamination is not large enough to cause such large rise in resistivity.

On the other hand, TiN films deposited at 425 °C and below exhibited an amorphous structure, which is significantly different from the polycrystalline structure observed for films grown at 500 °C. The lack of long-range crystalline periodicity in the amorphous structure leads to a much shorter mean free path for electron scattering, and hence results in appreciable increases in resistivity, as compared to a crystalline structure.<sup>19</sup> Accordingly, it is argued that the amorphous structure of the TiN films grown below 425 °C is the main contributor to the observed increase in film resistivity.

In this respect, target specifications published in the National Technology Roadmap for Semiconductors (NTRS) of the Semiconductor Industry Association (SIA) predict that overall effective via resistivity must remain below 2.0  $\mu\Omega \text{ cm}$  for devices with feature sizes between 0.50 and 0.18  $\mu\text{m}$ .<sup>20</sup> This number is predicted to be capped at 0.18  $\mu\Omega \text{ cm}$  for feature sizes below 0.18  $\mu\text{m}$ . It is thus suggested that the high resistivity TiN diffusion barrier technology might be viable in applications where aluminum liners are needed, given that in those cases, the resistivity of the diffusion barrier contributes only minimally to the total effective via stack resistivity. This is expected to occur quickly with the continued decrease in device feature size, wherein barrier layer thickness is predicted to shrink from  $\sim 21 \text{ nm}$  for 0.18  $\mu\text{m}$  devices, down to  $\sim 80 \text{ nm}$  for 0.05  $\mu\text{m}$  devices.

### 6. Effects of process parameters on conformality

Conformality and step coverage were found to be strongly dependent on source temperature within the process window investigated. Accordingly, our DOE studies were extended by performing an additional set of experiments, wherein the source temperature was varied between 120 and 200 °C, while all other process parameters were kept constant at their optimum values, including 400 °C substrate temperature, 50 sccm  $H_2$  carrier flow, 80 sccm  $M4$  reactant flow, 740 sccm  $H_2$  reactant flow, and 1.90 Torr reactor pressure.

Figure 12 displays the resulting correlation between step coverage and source temperature. In particular, the films deposited at 150 °C source temperature exhibited a



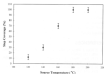


FIG. 12. Step coverage of CVD grown TaN films as a function of sinter temperature.

step coverage of less than 15%, while increasing sinter temperature above 180 °C improved the step coverage to better than 95%, as shown in the CB-SEM micrographs of a 0.6  $\mu\text{m}$ , 3.4:1 aspect ratio, and 0.30  $\mu\text{m}$ , 4.5:1 aspect ratio trench structures of, respectively, Figs. 13(a) and 13(b). The dependency of step coverage on sinter temperature could be attributed to the effects of the later on precursor vapor pressure and resulting precursor flux and partial pressure in the reaction zone. The increased precursor partial pressure at higher sinter temperature is expected to cause precursor saturation in the reaction zone, leading to improved step coverage.

In any case, it is clear that the thermal reaction of TaBr<sub>5</sub> with ammonia yields nitrogen-rich TaN films with high resistivity values. In this respect, our findings are similar to those reported by Tajima *et al.*<sup>20</sup> concerning the reaction mechanisms of tantalum pentachloride (TaCl<sub>5</sub>) and ammonia. Tajima reported that the reaction of TaCl<sub>5</sub> with NH<sub>3</sub> below 800 °C proceeds through the formation of a TaCl<sub>5</sub> · 5NH<sub>3</sub> intermediate. This intermediate subsequently reacts with ammonia to produce a Ta<sub>2</sub>N<sub>5</sub>-rich phase which exhibits high resistivity values. Given that TaBr<sub>5</sub> and TaCl<sub>5</sub> possess similar chemical characteristics and associated bonding configurations, it is suggested that the corresponding TaBr<sub>5</sub> decomposition pathway is identical to that for TaCl<sub>5</sub>, as follows:

Primary reactions:



Secondary reactions:



$$(x < 5).$$

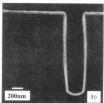
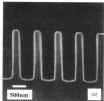
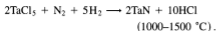


FIG. 13. CB-SEM micrographs for uniformity of CVD TaN films in 500 mTorr of (a) 0.6  $\mu\text{m}$ , 3.4:1 aspect ratio, and (b) 0.3  $\mu\text{m}$ , 4.5:1 aspect ratio trench structures.

In order to resolve this critical issue, an alternative CVD TaN process was explored by the present investigators by using N<sub>2</sub> and H<sub>2</sub> as co-reactants for the TaBr<sub>5</sub> system, instead of ammonia. This alternative is based on the work of Harber,<sup>1</sup> who studied the reaction of TaCl<sub>5</sub> with H<sub>2</sub> and N<sub>2</sub>. This work indicated that in this case, the decomposition process involved in the reaction of TaCl<sub>5</sub> with H<sub>2</sub> and N<sub>2</sub> leads to the formation of a low

resistivity TaN phase, as follows:



Based on these considerations, a low temperature (<450 °C) plasma-assisted CVD (PACVD) process was identified and developed by the present investigators. In this instance, the reaction of TaBr<sub>5</sub> with a (N<sub>2</sub> + H<sub>2</sub>) plasma produced the low resistivity cubic TaN phase. However, these findings are beyond the scope of this paper and will be presented in a subsequent report.

#### IV. SUMMARY AND CONCLUSIONS

A low temperature thermal CVD process was developed for the growth of TaN<sub>x</sub> thin films from the simple halide source, tantalum pentabromide (TaBr<sub>5</sub>) with ammonia and hydrogen as co-reactants. In the development of this process, a reaction kinetics study was first performed, indicating the existence of two sequential rate-controlling steps, with activation energy of reaction of 0.45 eV for the reaction rate-limited regime. A DOE approach was subsequently implemented to explore the effects of the four key process parameters, namely, substrate temperature, source temperature, hydrogen carrier gas flow, and ammonia reactant gas flow, on key film characteristics including growth rate, composition, resistivity, microstructure, and step coverage. The DOE was conducted using a response surface model which included quadratic terms and was generated from a CCF design. The resulting findings indicated that a wide CVD process window exists for the low temperature deposition of nitrogen-rich amorphous TaN<sub>x</sub> with C, O, and Br contamination levels below 1 at.%. Conformality was higher than 95% in nominally 0.3 μm, 4.5:1 aspect ratio structures. However, film resistivities were high across the entire parameter space investigated.

Our findings were consistent with previous reaction mechanism studies which indicated that the insulating Ta<sub>3</sub>N<sub>5</sub> phase is the major product of the TaCl<sub>5</sub>-NH<sub>3</sub> reaction. In this respect, it is suggested that the high resistivity TaN<sub>x</sub> diffusion barrier might be viable for device applications that require ultrathin liner, given that in this case, the resistivity of the liner represents only a minor contribution to the total effective via stack resistivity. Otherwise, a PACVD approach, which employs TaBr<sub>5</sub>, N<sub>2</sub>, and H<sub>2</sub> co-reactants, provides an alternative route to the growth of the low resistivity cubic TaN phase.<sup>21</sup>

#### ACKNOWLEDGMENTS

The work was partially supported by the Semiconductor Research Corporation (SRC) Center for Advanced Interconnect Science and Technology (CAIST) and the New York State Center for Advanced Thin Film Technology (CAT). This support is gratefully acknowledged.

#### REFERENCES

1. T. Nitta, T. Ohmi, S. Sakai, and T. Shibata, *J. Electrochem. Soc.* **140**, 1131 (1993).
2. G. P. Rao, *Multilevel Interconnect Technology* (McGraw-Hill, Inc., New York, 1994).
3. M. Takeyama, A. Noya, T. Sase, and A. Ohta, *J. Vac. Sci. Technol.* **B14**, 674 (1996).
4. E. Kobeda, J. Warnock, J. Gambino, S. Brosky, and S. Basavaiah, *J. Appl. Phys.* **72**, 2743 (1992).
5. *CRC Handbook of Chemistry and Physics*, 71st ed., edited by J. Lide (CRC Press, Cleveland, OH, 1991), pp. 4–109.
6. J. S. Reid, E. Kolawa, and M. Nicolet, *J. Mater. Res.* **7**, 2424 (1992).
7. K. Holloway, P. M. Fryer, C. Cabral, and P. J. Bailey, *J. Appl. Phys.* **71**, 5433 (1992).
8. K. Hieber, *Thin Solid Films* **24**, 157 (1974).
9. R. Fix, R. Gordon, and D. Hoffman, *Chem. Mater.* **5**, 614 (1993).
10. H. Chiu and W. Chang, *J. Mater. Sci. Lett.* **11**, 92 (1992).
11. M. Tsai, *Appl. Phys. Lett.* **67**, 1129 (1995).
12. I. Barin, O. Knacke, and O. Kubaschewski, *Thermochemical Properties of Inorganic Substances Supplement* (Springer-Verlag, Berlin, Heidelberg, New York, 1977).
13. M. Seel and P. S. Bagus, *Phys. Rev.* **B28**, 2023 (1983).
14. C. Faltermeyer, C. Goldberg, M. Jones, A. Upham, D. Manger, G. Peterson, J. Lau, and A. Kaloyeros, *J. Electrochem. Soc.* **144**, 1002 (1997).
15. See, for example, A. Knorr, R. Talevi, H. Gundlach, K. A. Kumar, G. P. Peterson, A. E. Kaloyeros, J. J. Sullivan, and J. Loan, *J. Vac. Sci. Technol.* **B15**, 1758 (1997); and X. Chen, *Tantalum and Tantalum Nitride Films Grown by Inorganic Low Temperature Chemical Vapor Deposition for Copper Metallization: Chemistry, Process, and Material Development and Characterization* (Doctoral Thesis, The University at Albany-SUNY Press, Albany, New York, 1998).
16. J. Moulder, W. Stickle, P. Sobol, and K. Bomken, Perkin-Elmer Corporation, Eden Prairie, MN (1992).
17. L. Toth, *Transition Metal Carbides and Nitrides* (Academic Press, New York, 1971), p. 188.
18. S. P. Murarka, *Metallization: Theory and Practice for VLSI and ULSI* (Butterworth-Heinemann, March 1993).
19. The National Technology Roadmap for Semiconductors (Semiconductor Research Association, San Jose, CA, 1997), pp. 99–113.
20. A. Yajima, R. Matsuzaki, and Y. Saeki, *Denki Kagaku* **51**, 676 (1983).
21. X. Chen, G. G. Peterson, G. Nuesca, H. L. Frisch, A. E. Kaloyeros, and B. Arkles, unpublished.